Current Profile Optimization for Combined State of Charge and State of Health Estimation of Lithium Ion Battery Based on Cramer–Rao Bound Analysis

Ziyou Song, *Member, IEEE*, Xiaogang Wu, Xuefeng Li, Jing Sun, *Fellow, IEEE*, Heath F. Hofmann, *Senior Member, IEEE*, and Jun Hou, *Member, IEEE*

***Abstract*—Online State of Charge (SoC) and State of Health (SoH) estimations are essential for efficient, safe, and reliable operation of Lithium ion batteries. Based on the first-order equivalent-circuit model (ECM), a multi-scale extended Kalman filter is adopted in this paper to estimate ECM parameters and battery SoC using dual time scales. The nature of the battery excitations significantly influences the estimation performance. When the input–output data, i.e., the input current and output voltage, is insufficiently rich in frequency content, the estimation performance is poor. Thus, the excitation current should be optimized for the accurate estimation of parameters and states. A Cramer–Rao bound analysis is conducted considering voltage noise, current amplitude, and current frequency, which shows the loss of accuracy in multi-parameter estimation (estimating all states and parameters) when compared to single-parameter estimation (estimating only one parameter/state). However, it also shows that the loss of accuracy can be significantly reduced when the excitation current is carefully chosen to satisfy certain criteria. Both simulation and experimental results verify the analysis results and show that a current profile with optimal frequency components achieves the best estimation performance, thereby, providing guidelines for designing battery current profiles for improved SoC and SoH estimation performance.**

***Index Terms*—Cramer–Rao (CR) bound, current profile design, estimation accuracy, lithium ion battery, multi-scale extended Kalman filter (EKF), State of Charge/State of Health (SoC/SoH) estimation.**

I. Introduction

LITHIUM-ion batteries have relatively high energy density, high power density, long life, and low environmental impact, hence they have been widely used in consumer electronics, electric vehicles, and grid storage applications [1]. Accurate estimation of critical battery states, such as the State of Charge (SoC) and State of Health (SoH), play an important role in ensuring safe, reliable, and efficient operation [2]. State estimation and parameter estimation are tightly interconnected when model-based approaches are used [3]. Commonly used models for SoC and SoH estimations include the open-circuit voltage (OCV) model [4], neural-network model [5], equivalent-circuit model (ECM) [6], and electrochemical model [7]. ECM has been extensively investigated for battery monitoring and management due to its simplicity and adequate fidelity in many applications [8].

For SoC estimation, the basic approach is Coulomb counting, where the battery current is numerically integrated over time to quantify the change of stored charge [9]. However, this open-loop method does not provide sufficient accuracy for practical applications, as it is sensitive to initial SoC error and measurement noise [10]. Other approaches include, but are not limited to extended Kalman filter (EKF) [11], unscented Kalman filter [12], H_∞ observer [13], sliding mode observer [14], and fuzzy-logic-based method [15]. The above estimation methods require knowledge of battery parameters, which is often acquired via offline measurement or identification. As a result, variations in the battery model parameters caused by aging and changes in operating conditions can lead to performance degradation [16]. SoH reflects the battery health state, and is generally defined as the ratio of the remaining capacity to the original capacity [17]. The estimation of battery capacity (i.e., SoH) and other parameters can be conducted independently from SoC estimation. SoH estimation algorithms, including Kalman filters [18], least-squares methods [19], moving-horizon observers [20], and Lyapunov-based methods [21] can be found in the literature. The influence of battery degradation and operating condition changes should be considered in SoC/SoH estimation [16], motivating the investigation of the combined estimation of SoC and SoH. For example, the standard dual EKF (DEKF) has been developed to identify SoC and SoH simultaneously [22]. The multi-scale DEKF uses a "slow" time scale to calculate battery parameters and a "fast" time scale to calculate SoC [23]. This dual estimation method lowers the computational cost [16], thus it is also employed in this paper.

Manuscript received June 11, 2018; revised September 10, 2018; accepted October 17, 2018. Date of publication October 21, 2018; date of current version May 2, 2019. The work of Z. Song, J. Sun, H. Hofmann, and J. Hou was supported by the Office of Naval Research under Grant N00014-16-1-3108. *(Corresponding author: Jun Hou.)*

Z. Song and J. Sun are with the Department of Naval Architecture and Marine Engineering, University of Michigan, Ann Arbor, MI 48109 USA (e-mail: ziyou.songthu@gmail.com; jingsun@umich.edu).

X. Wu and X. Li are with College of Electrical and Electronics Engineering, Harbin University of Science and Technology, Harbin 150080, China (e-mail: xgwu@hrbust.edu.cn; lixuefeng_ma16@hrbust.edu.cn).

H. Hofmann and J. Hou are with the Department of Electrical Engineering and Computer Science, University of Michigan, Ann Arbor, MI 48109 USA (e-mail: hofmann@umich.edu; junhou@umich.edu).

Color versions of one or more of the figures in this paper are available online at http://ieeexplore.ieee.org.

Digital Object Identifier 10.1109/TPEL.2018.2877294

In addition to the estimation algorithm, the input–output data used in the estimation process, i.e., the battery current and voltage, also affects the estimation accuracy [24]. A persistently exciting (PE) input condition must be satisfied to guarantee the convergence of the estimated parameters. Generally, the input signal should contain one frequency component for every two estimated parameters [25]. For all the works mentioned above, the data is used in the estimation without analyzing whether it is sensitive to the parameters/states. Furthermore, the noise and bias of the sensors (voltage and current sensors) cause errors in battery state and parameter estimation, and these errors are enlarged when insufficiently rich data is used [24].

The impact of data on the estimation quality has previously been studied analytically in [24] and [26] considering parameter sensitivity, the Fisher information matrix, and the Cramer–Rao (CR) bound. These references provide guidelines on data selection by exploring the fundamental relationship between estimation accuracy and measurement data. Similarly, Rothenberger *et al.* optimized the battery cycling current to maximize the Fisher information matrix for a nonlinear second-order model of a lithium-ion battery cell [27], [28]. Klintberg *et al.* computed the posterior CR lower bounds numerically to quantify the accuracy of Bayesian estimators [26]. Lin *et al.* derived analytic bounds on the estimation accuracy of SoC, capacity, and ohmic resistance under various circumstances [29]. SoC estimation error considering sensor bias [30], model inaccuracy [31], and algorithms are also investigated. However, the current profile optimization for the simultaneous estimation of all battery states and parameters, which is more complex than the problems addressed in above papers, has not been investigated.

In this paper, the sinusoidal current excitations are adopted. Considering voltage noise, current amplitude, and current frequency, the CR bounds on the estimation accuracy of SoC, SoH, and the ECM parameters are derived using the time-averaged Fisher information matrix. Results show a loss of accuracy in combined estimation where all states and parameters are estimated simultaneously when compared to single-parameter estimation where only one parameter or state is estimated (the other parameters and states are assumed to be well-known). In addition, the CR bound analysis result shows that the estimation accuracy of combined estimation can be significantly improved when the battery current contains optimal frequency components, although different states and parameters may inherently require different excitation frequencies. The analysis is verified using both simulation and experimental results, focusing on the Samsung 18 650 Lithium ion battery. By carefully designing the current profile, estimation accuracy and reliability can be significantly improved. The conclusions in this paper can be directly used to design offline experiments for estimation. In addition, for the over-actuated systems, such as a battery/supercapacitor hybrid energy storage system, the method can provide guidelines for optimizing the battery current waveform online to improve the estimation performance when battery states and parameters need to be updated simultaneously [32].

To the best of our knowledge, this is the first paper investigating current waveform design for simultaneous parameter and state estimation of Lithium ion batteries to improve the estimation accuracy. The rest of this paper is organized as follows. In Section II, the battery model and the DEKF are introduced. In Section III, CR bounds of battery states and parameters are derived for both single-parameter and multi-parameter estimation scenarios. In Section IV, a current profile is designed to improve the estimation performance, and is validated through simulation. In Section V, experimental results are provided for verification. Some conclusions are given in Section VI.

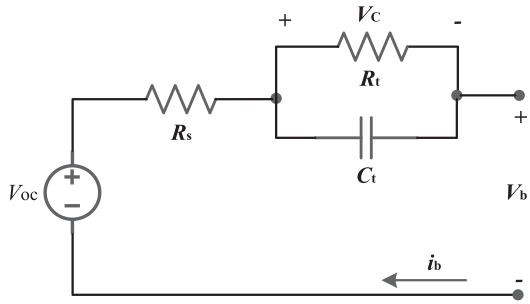

Fig. 1. First-order ECM of battery.

II. Combined Estimation of SoC and SoH

A. Estimation Problem Description

The first-order ECM adopted in this paper is shown in Fig. 1, where an ohmic resistor with resistance R_s, a parallel RC pair $(R_t//C_t)$, and a dc source with voltage $V_{\rm oc}$ are connected in series [33]. The battery terminal voltage is defined as V_b and the battery current is defined as i_b (positive for discharging and negative for charging). We point out that, when compared to the first-order ECM used in this paper, higher order models (e.g., 2RC and 3RC circuit models as well as the electrochemical model) can represent the battery dynamics more accurately. However, there is a tradeoff between model accuracy and computational cost. When compared to the first-order circuit model, the parameter estimation of higher order models has much higher computational cost and a more critical requirement on the battery current waveform. For example, when the second-order ECM is adopted, there are seven parameters to be identified, consequently four sinusoidal current components are required to persistently excite the battery [25], which is hard to realize in practical applications. In addition, the CR bound analysis, which will be shown in Section III, becomes very complex since more parameters are involved in the estimation process for high-order models, meaning that it is difficult to determine and implement the optimal current waveform for higher order models. As a result, the choice of the model is the result of a tradeoff between accuracy and simplicity. We note that the proposed algorithm can be directly generalized for higher order ECMs by following the same procedures provided in this paper.

According to Kirchhoff's laws, the ECM dynamics can be presented as follows:

$$\begin{cases} \dot{V}_C = -\frac{1}{C_t R_t} V_C + \frac{1}{C_t} i_b \\ V_b = V_{\rm OC} - R_s i_b - V_C \end{cases} \tag{1}$$

where V_C is the voltage across the RC pair, which cannot be measured in experiments. The OCV-SoC curve can be expressed as [34]

$$V_{\mathrm{OC}}(z) = K_0 - \frac{K_1}{z} - K_2 z + K_3 \ln(z) + K_4 \ln(1-z) \quad (2)$$

where K_{0-4} are the model parameter and z is the normalized SoC (from 0 to 1). The SoC under load can be modeled as [35]

$$z = z_0 - \int_{t_0}^{t} \frac{\eta}{Q_b} i_b(t) dt \quad (3)$$

where z_0 is the initial SoC, η is the charge/discharge efficiency, t_0 is the initial time, t is the time, and Q_b is the battery capacity. The coefficients K_{0-4} in the OCV-SoC relationship do not significantly change with different battery degradation levels and operating conditions, as verified by previous research [36], [37]. This means that the OCV can be accurately estimated by (2) as long as the true SoC can be provided. The battery capacity Q_b and the parameters R_s, R_t, and C_t in the ECM are significantly influenced by battery degradation and/or the operating condition. It is difficult to calibrate these parameters offline over all battery degradation levels and operating conditions. Thus, these parameters, which directly influence SoC and SoH estimations, need to be estimated when the operating condition dramatically changes (e.g., temperature) [38].

In this paper, the estimation problem involves two states (i.e., the RC pair voltage V_C and the SoC z) and four parameters (i.e., ohmic resistance R_s, diffusion resistance R_t, time constant $\tau = R_t C_t$, and battery capacity Q_b). Based on (1)– (3), the general discrete time state-space equation for the multi-scale EKF can be expressed as follows [16]:

$$\begin{cases} \boldsymbol{\theta}_{k+1} = \boldsymbol{\theta}_k + \mathbf{r}_k \\ \mathbf{X}_{k,l+1} = \mathbf{H}\left(\mathbf{X}_{k,l}, \boldsymbol{\theta}_k, u_{k,l}\right) + \mathbf{w}_{k,l} \\ Y_{k,l+1} = \mathbf{G}\left(\mathbf{X}_{k,l}, \boldsymbol{\theta}_k, u_{k,l}\right) + v_{k,l} \end{cases} \quad (4)$$

where

$$\boldsymbol{\theta}_k = \begin{bmatrix} R_s(k) \\ R_t(k) \\ \tau(k) \\ 1/Q_b(k) \end{bmatrix}, \mathbf{X}_{k,l} = \begin{bmatrix} V_C(k,l) \\ z(k,l) \end{bmatrix},$$

$$u_{k,l} = i_b(k,l), Y_{k,l+1} = V_b(k,l+1)$$

$$\begin{cases} \mathbf{H}\left(\mathbf{X}_{k,l}, \boldsymbol{\theta}_k, u_{k,l}\right) = \begin{bmatrix} e^{-\frac{T}{\tau}} & 0 \\ 0 & 1 \end{bmatrix} \mathbf{X}_{k,l} + \begin{bmatrix} R_t\left(1 - e^{-\frac{T}{\tau}}\right) \\ -\frac{\eta T}{Q_b} \end{bmatrix} u_{k,l} \\ \mathbf{G}(\mathbf{X}_{k,l}, \boldsymbol{\theta}_k, u_{k,l}) = \mathrm{OCV}(z(k,l)) - V_C(k,l) - R_s(k) u_{k,l} \end{cases}$$

k and l are the two time-scale indices, T is the sampling period (i.e., 1 s), $\mathbf{X}_{k,l}$ is the state vector at the time $t_{k,l}$, $\boldsymbol{\theta}_k$ is the parameter vector at the time $t_{k,0}$, $u_{k,l}$ is the system input, $Y_{k,l}$ is the system output, $\mathbf{r}_k$ is the process noise for parameters, $\mathbf{w}_{k,l}$ is process noise for states, and $v_{k,l}$ is the measurement noise. The relationship between the two time scales is given by

$$t_{k,l} = t_{k,0} + l \times T, 1 \le l \le L \quad (5)$$

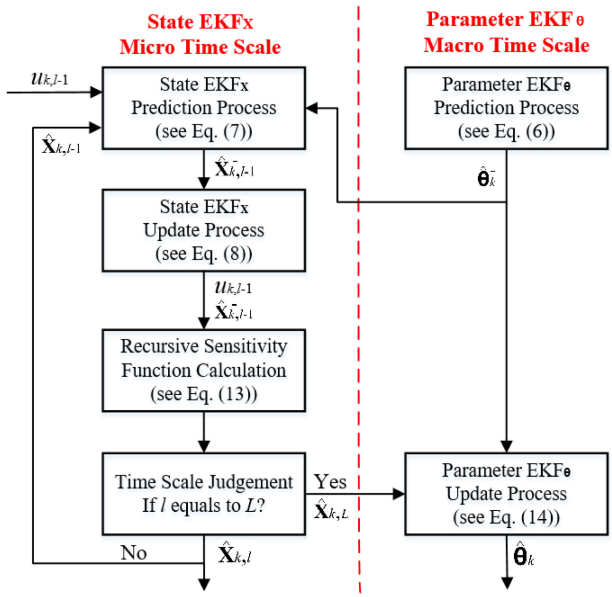

Fig. 2. Flowchart of the multi-scale EKF.

where L represents the time-scale separation ratio, and $\mathbf{X}_{k,0} = \mathbf{X}_{k-1,L}$. In Section II-B, the dual EKF is designed to estimate $\mathbf{X}$ and θ simultaneously based on input u and output Y.

B. Review of Multi-Scale EKFs

The multi-scale EKF is developed based on the standard dual EKF method, which is a commonly used technique for simultaneous estimation of battery states and parameters [39]. For the dual EKF, two EKFs are run concurrently and, at every time step when the observation is available, the state EKF estimates the states using the latest model parameter estimates from the parameter EKF, while the parameter EKF estimates the model parameters using the latest state estimates from the state EKF [23]. The standard dual EKF estimates both states and parameters on the same time scale. However, for systems like batteries, given the physical time-scale separation, it is desirable to estimate the slowly time-varying parameters on the macrotime-scale while estimating the fast time-varying states on the microtime-scale [39], which can reduce computational effort and provide more stable estimates [16], [23], [39]. The flowchart of the adopted multi-scale EKF is depicted in Fig. 2, and the detailed information is provided in [16].

III. CR Lower Bounds for Battery Parameters and States

Although the estimation method is important, the influence of the battery current waveform (i.e., the input) on the estimation performance is also significant. The relationship between the estimation accuracy and the data is quantitatively investigated in this section. The CR bound, which indicates the lower bound of the estimation error covariance of unbiased estimation, can be used to quantify the estimation accuracy [40]. A sinusoidal current is adopted in this paper, and the CR bounds of the battery parameters and states are derived using Laplace transforms.

A. Process for Calculating Time-Averaged CR Bound

The process for computing the time-averaged CR bound is introduced in this section. V_C is not considered in the CR bound analysis for simplification, since it highly depends on R_t and τ. Assume the battery voltage $V_b(t)$ and current $i_b(t)$ are measured continuously and used to estimate a parameter vector $\boldsymbol{\theta} = [\theta_1, \theta_2, \ldots, \theta_m]^{\mathrm{T}}$. The relationship between input $i_b(t)$ and output $V_b(t)$ in the frequency domain assumes the generic form

$$V_b(s) = J[\boldsymbol{\theta}, i_b(s)] \tag{6}$$

where s is the complex Laplace variable. The sensitivity of the output to parameter θ_i is defined as

$$\frac{\partial V_b}{\partial \theta_i}(s) = \frac{\partial J[\boldsymbol{\theta}, i_b(s)]}{\partial \theta_i}. \tag{7}$$

The sensitivity in the time domain can be expressed using the inverse Laplace transform $\mathcal{L}^{-1}$

$$\frac{\partial V_b}{\partial \theta_i}(t) = \mathcal{L}^{-1}\left[\frac{\partial V_b}{\partial \theta_i}(s)\right]. \tag{8}$$

Considering Gaussian noise in the voltage measurement, when the periodic input (with a period of T_i) is used, the time-averaged Fisher Matrix $\bar{\mathbf{F}}_c$ can be calculated as [24]

$$\bar{\mathbf{F}}_c = \frac{1}{\sigma_V^2}\frac{1}{T_i}\begin{bmatrix} \int_0^{T_i}\left(\frac{\partial V_b}{\partial \theta_1}\right)^2 dt & \int_0^{T_i}\frac{\partial V_b}{\partial \theta_1}\frac{\partial V_b}{\partial \theta_2}dt & \cdots & \int_0^{T_i}\frac{\partial V_b}{\partial \theta_1}\frac{\partial V_b}{\partial \theta_m}dt \\ \int_0^{T_i}\frac{\partial V_b}{\partial \theta_2}\frac{\partial V_b}{\partial \theta_1}dt & \int_0^{T_i}\left(\frac{\partial V_b}{\partial \theta_2}\right)^2 dt & \cdots & \int_0^{T_i}\frac{\partial V_b}{\partial \theta_2}\frac{\partial V_b}{\partial \theta_m}dt \\ \vdots & \vdots & \vdots & \vdots \\ \int_0^{T_i}\frac{\partial V_b}{\partial \theta_m}\frac{\partial V_b}{\partial \theta_1}dt & \int_0^{T_i}\frac{\partial V_b}{\partial \theta_m}\frac{\partial V_b}{\partial \theta_2}dt & \cdots & \int_0^{T_i}\left(\frac{\partial V_b}{\partial \theta_m}\right)^2 dt \end{bmatrix} \tag{9}$$

where the overbar symbol ($^-$) denotes a time-averaged value and σ_V^2 is the variance of the voltage measurement noise. The CR bound can be obtained by inverting the Fisher Matrix [41]

$$\mathrm{var}(\theta_i) \geq \underline{\sigma}^2(\theta_i) = \mathrm{diag}\left(\bar{\mathbf{F}}_c^{-1}\right)_i \tag{10}$$

where $\mathrm{var}(\theta_i)$ is the variance of the estimation error for θ_i, $\underline{\sigma}^2(\theta_i)$ is the CR lower bound of θ_i, which represents the minimum achievable variance of the estimation error for θ_i, and $\mathrm{diag}(\bar{\mathbf{F}}_c^{-1})_i$ is the ith diagonal element of $\bar{\mathbf{F}}_c^{-1}$. This paper focuses on the cases when $m = 1$ (i.e., single-parameter estimation) and $m = 5$ (i.e., multi-parameter estimation).

B. CR Lower Bound Derivation for Single-Parameter Estimation

To derive the transfer function from i_b to V_b, several assumptions are given as follows:

1) The initial value of V_C is assumed to be 0.
2) The variations of R_s, R_t, and τ with respect to time are neglected in the estimation process [42].

Based on (1), the transfer function can be derived using the Laplace transform

$$V_b(s) = V_{\mathrm{OC}}(s) - R_s i_b(s) - \frac{R_t}{1+\tau s} i_b(s). \tag{11}$$

The OCV-SoC is characterized by (2). It has been proven the slope of the OCV-SoC curve is constant for most battery chemistries within the normal operation range. For example, the OCV slope is nearly constant in the range of 10%–90% SoC, e.g., 0.65 V/100% for a LiNiMnCo battery and 0.17 V/100% for a $LiFePO_4$ battery [6], [43]. As a result, (2) is linearized to simplify the CR bound analysis

$$V_{\mathrm{OC}}(t) = a\left(z_0 - \int_{t_0}^{t}\frac{\eta i_b(\upsilon)}{Q_b}d\upsilon\right) + b \tag{12}$$

where a and b are the coefficients of the linearized OCV-SoC function, and ν is the integration variable. It has been proven that the OCV-SoC relationship does not significantly change with different battery degradation levels and operating conditions [36], [37], therefore, a and b can be treated as known constants. As shown in (12), the errors in initial SoC (i.e., z_0) and the battery capacity Q_b will induce significant estimation errors in the SoC and battery terminal voltage. Based on (11) and (12), we have

$$V_b(s) = \frac{az_0}{s} - \frac{a}{s}\frac{\eta}{Q_b}i_b(s) + \frac{b}{s} - R_s i_b(s) - \frac{R_t}{1+\tau s}i_b(s). \tag{13}$$

The CR bound analysis is based on (13). In this section, we consider the single-parameter estimation where only one parameter/state is estimated, while the other states/parameters are assumed to be known. The sensitivity of the output (i.e., battery terminal voltage) to the estimated state/parameter can be derived in the frequency domain according to (7)

$$\begin{aligned} &\frac{\partial V_b}{\partial z_0}(s) = \frac{a}{s},\ \frac{\partial V_b}{\partial R_s}(s) = -i_b(s),\ \frac{\partial V_b}{\partial R_t}(s) = -\frac{1}{1+\tau s}i_b(s) \\ &\frac{\partial V_b}{\partial \tau}(s) = \frac{R_t s}{(1+\tau s)^2}i_b(s),\ \ \frac{\partial V_b}{\partial (1/Q_b)}(s) = -\frac{a\eta}{s}i_b(s). \end{aligned} \tag{14}$$

We consider a sinusoidal current input

$$\begin{cases} i_b(t) = M\cos(\omega t) \\ i_b(s) = \frac{Ms}{s^2+\omega^2} \end{cases} \tag{15}$$

where M is the current magnitude and ω is the current frequency. Using (15) in (14), and taking the inverse Laplace transform L^{-1}, the sensitivities for z_0, R_s, and $1/Q_b$ can be easily derived as

$$\begin{cases} \dfrac{\partial V_b}{\partial z_0}(t) = L^{-1}\left\{\dfrac{a}{s}\right\} = a \\ \dfrac{\partial V_b}{\partial R_s}(t) = L^{-1}\{-i_b(s)\} = -M\cos(\omega t) \\ \dfrac{\partial V_b}{\partial (1/Q_b)}(t) = L^{-1}\left\{-\dfrac{a\eta}{s}i_b(s)\right\} = -\dfrac{Ma\eta\sin(\omega t)}{\omega}. \end{cases} \tag{16}$$

For R_t and τ, the sensitivity expressions are relatively complex. Specifically, for R_t, based on (14) and (15), we have

$$\frac{\partial V_b}{\partial R_t}(t) = L^{-1}\left\{-\frac{1}{1+\tau s} i_b(s)\right\} = \frac{M\, e^{-\frac{t}{\tau}}}{1+\omega^2\tau^2} - \frac{M\cos(\omega t) + M\omega\tau\sin(\omega t)}{1+\omega^2\tau^2}. \quad (17)$$

As $t \to \infty$, (17) asymptotically converges to

$$\frac{\partial V_b}{\partial R_t}(t) \to -\frac{M\cos(\omega t) + M\omega\tau\sin(\omega t)}{1+\omega^2\tau^2}. \quad (18)$$

Similarly, for τ, the asymptotic sensitivity can be given as

$$\frac{\partial V_b}{\partial \tau}(t) \to -\frac{MR_t\omega\left[\omega^2\tau^2\sin(\omega t) - \sin(\omega t) + 2\omega\tau\cos(\omega t)\right]}{\left(1+\omega^2\tau^2\right)^2}. \quad (19)$$

Based on (16), (18), and (19), the time-averaged Fisher Matrices for z_0, R_s, R_t, τ, and $1/Q_b$ can be calculated according to (9)

$$\begin{cases} \bar{\mathbf{F}}(z_0) = \frac{1}{\sigma_V^2}\frac{\omega}{2\pi}\int_0^{\frac{2\pi}{\omega}}\left[\frac{\partial V_b}{\partial z_0}(t)\right]^2 dt = \frac{a^2}{\sigma_V^2} \\ \bar{\mathbf{F}}(R_s) = \frac{1}{\sigma_V^2}\frac{\omega}{2\pi}\int_0^{\frac{2\pi}{\omega}}\left[\frac{\partial V_b}{\partial R_s}(t)\right]^2 dt = \frac{M^2}{2\sigma_V^2} \\ \bar{\mathbf{F}}(R_t) = \frac{1}{\sigma_V^2}\frac{\omega}{2\pi}\int_0^{\frac{2\pi}{\omega}}\left[\frac{\partial V_b}{\partial R_t}(t)\right]^2 dt = \frac{M^2}{2\sigma_V^2(1+\omega^2\tau^2)} \\ \bar{\mathbf{F}}(\tau) = \frac{1}{\sigma_V^2}\frac{\omega}{2\pi}\int_0^{\frac{2\pi}{\omega}}\left[\frac{\partial V_b}{\partial \tau}(t)\right]^2 dt = \frac{M^2R_t^2\omega^2}{2\sigma_V^2(1+\omega^2\tau^2)^2} \\ \bar{\mathbf{F}}(1/Q_b) = \frac{1}{\sigma_V^2}\frac{\omega}{2\pi}\int_0^{\frac{2\pi}{\omega}}\left[\frac{\partial V_b}{\partial (1/Q_b)}(t)\right]^2 dt = \frac{M^2a^2\eta^2}{2\sigma_V^2\omega^2}. \end{cases} \quad (20)$$

Consequently, the time-averaged CR bounds can be obtained as follows:

$$\begin{cases} \bar{\sigma}(z_0) = \bar{\mathbf{F}}(z_0)^{-\frac{1}{2}} = \frac{\sigma_V}{a} \\ \bar{\sigma}(R_s) = \bar{\mathbf{F}}(R_s)^{-\frac{1}{2}} = \frac{\sqrt{2}\sigma_V}{M} \\ \bar{\sigma}(R_t) = \bar{\mathbf{F}}(R_t)^{-\frac{1}{2}} = \frac{\sqrt{2}\sigma_V\sqrt{1+\omega^2\tau^2}}{M} \\ \bar{\sigma}(\tau) = \bar{\mathbf{F}}(\tau)^{-\frac{1}{2}} = \frac{\sqrt{2}\sigma_V\left(1+\omega^2\tau^2\right)}{MR_t\omega} \\ \bar{\sigma}(1/Q_b) = \bar{\mathbf{F}}(1/Q_b)^{-\frac{1}{2}} = \frac{\sqrt{2}\sigma_V\omega}{Ma\eta}. \end{cases} \quad (21)$$

Based on (21), several remarks for single-parameter estimation can be obtained.

Remark 1: As expected, reducing the noise in voltage measurement would lead to improved estimation accuracy. But this is generally limited by the voltage sensor performance.

Remark 2: The SoC estimation is not influenced by the current and only related to the OCV slope a. The accuracy of estimated SoC can be improved with a larger OCV slope because it makes the SoC more detectable from the battery terminal voltage, and this conclusion is also given in [24].

Remark 3: The estimation accuracy of R_s, R_t, τ, and $1/Q_b$ can be improved by increasing the current amplitude. The estimation of R_s is not influenced by the current frequency.

Remark 4: The current frequency ω should be as small as possible to increase the estimation accuracy of R_t. In addition, the CR bound of τ achieves the minimum value $\frac{2\sqrt{2}\sigma_V\tau}{MR_t}$ when $\omega = \frac{1}{\tau}$.

Remark 5: The estimation accuracy of $1/Q_b$ can be improved by decreasing the current frequency. When ω is 0, the input is a direct current with amplitude of M, which is the best case to estimate $1/Q_b$. The reason is that the battery capacity influences the output (i.e., battery terminal voltage) via the SoC variation, and only a large SoC variation can lead to a detectable voltage change given the relatively small OCV-SoC slope.

C. CR Lower Bound Derivation for Multi-Parameter Estimation

When z_0, R_s, R_t, τ, and $1/Q_b$ are estimated simultaneously, the error variance will be no less than that of single-parameter estimation, as shown in [24] and [29]. The estimation processes of different states/parameters will influence each other, which involves substantial uncertainties in the estimation. Based on (9), (16), (18), and (19), the time-averaged Fisher matrix $\bar{\mathbf{F}}_{c5}$ for multi-parameter estimation can be derived as

$$\bar{\mathbf{F}}_{c5} = \begin{bmatrix} \frac{a^2}{\sigma_V^2} & \mathbf{0} \\ \mathbf{0} & \bar{\mathbf{F}}_{c4} \end{bmatrix} \quad (22)$$

where $\bar{\mathbf{F}}_{c4}$ is the time-averaged Fisher matrix for the multi-parameter estimation of R_s, R_t, τ, and $1/Q_b$, and is given by (23) shown at the bottom of this page.

It can be seen that the CR bound of SoC only depends on the measurement noise and OCV slope, which is the same as in the case of single-parameter estimation. This means that the SoC estimation is not influenced by other parameters. As a result, we will focus on the multi-parameter estimation of R_s, R_t, τ, and $1/Q_b$. Similar to single-parameter estimation, the estimation accuracy for multi-parameter estimation is proportional to the noise level in the voltage measurement. Following the general rule that one frequency component is needed for every two unknown parameters [25], a current waveform with two sinusoidal components is considered. To simplify the problem, we consider the two sinusoidal signals to have the same amplitudes and with frequencies ω and 5ω, i.e.,

$$i_b(t) = M\cos(\omega t) + M\cos(5\omega t) \quad (24)$$

$$\bar{\mathbf{F}}_{c4} = \frac{1}{\sigma_V^2}\frac{\omega}{2\pi}\begin{bmatrix} \int_0^{\frac{2\pi}{\omega}}\left(\frac{\partial V_b}{\partial R_s}\right)^2 dt & \int_0^{\frac{2\pi}{\omega}}\frac{\partial V_b}{\partial R_s}\frac{\partial V_b}{\partial R_t}dt & \int_0^{\frac{2\pi}{\omega}}\frac{\partial V_b}{\partial R_s}\frac{\partial V_b}{\partial \tau}dt & \int_0^{\frac{2\pi}{\omega}}\frac{\partial V_b}{\partial R_s}\frac{\partial V_b}{\partial (1/Q_b)}dt \\ \int_0^{\frac{2\pi}{\omega}}\frac{\partial V_b}{\partial R_t}\frac{\partial V_b}{\partial R_s}dt & \int_0^{\frac{2\pi}{\omega}}\left(\frac{\partial V_b}{\partial R_t}\right)^2 dt & \int_0^{\frac{2\pi}{\omega}}\frac{\partial V_b}{\partial R_t}\frac{\partial V_b}{\partial \tau}dt & \int_0^{\frac{2\pi}{\omega}}\frac{\partial V_b}{\partial R_t}\frac{\partial V_b}{\partial (1/Q_b)}dt \\ \int_0^{\frac{2\pi}{\omega}}\frac{\partial V_b}{\partial \tau}\frac{\partial V_b}{\partial R_s}dt & \int_0^{\frac{2\pi}{\omega}}\frac{\partial V_b}{\partial \tau}\frac{\partial V_b}{\partial R_t}dt & \int_0^{\frac{2\pi}{\omega}}\left(\frac{\partial V_b}{\partial \tau}\right)^2 dt & \int_0^{\frac{2\pi}{\omega}}\frac{\partial V_b}{\partial \tau}\frac{\partial V_b}{\partial (1/Q_b)}dt \\ \int_0^{\frac{2\pi}{\omega}}\frac{\partial V_b}{\partial (1/Q_b)}\frac{\partial V_b}{\partial R_s}dt & \int_0^{\frac{2\pi}{\omega}}\frac{\partial V_b}{\partial (1/Q_b)}\frac{\partial V_b}{\partial R_t}dt & \int_0^{\frac{2\pi}{\omega}}\frac{\partial V_b}{\partial (1/Q_b)}\frac{\partial V_b}{\partial \tau}dt & \int_0^{\frac{2\pi}{\omega}}\left(\frac{\partial V_b}{\partial (1/Q_b)}\right)^2 dt. \end{bmatrix} \quad (23)$$

TABLE I
SPECIFICATIONS FOR THE 18 650 BATTERY CELL

Parameter	Value
Nominal Voltage (V)	3.63
Cell Capacity (Ah)	2.47
Cell Weight (g)	45
Current Limitations of Charge and Discharge (A)	-2.6/5.2
Ohmic Resistance R_s (mΩ)	~100
Diffusion Resistance R_t (mΩ)	~30
Time Constant τ (s)	~15
Discharge/Charge Efficiency η (%)	98
OCV-SoC slope a (mV/100%)	~8.845
Standard Deviation of Voltage Measurement Noise σ_V (mV)	20
Battery Current Amplitude M (A)	1

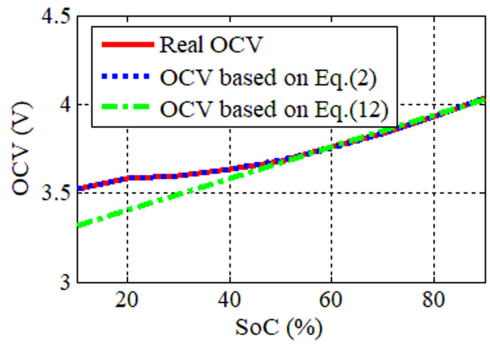

Fig. 3. OCV-SoC curve.

which has the following Laplace transform:

$$i_b(s) = \frac{Ms}{s^2+\omega^2} + \frac{Ms}{s^2+25\omega^2}. \tag{25}$$

The time-averaged Fisher matrix for this current waveform is complicated. Moreover, it is difficult to derive closed-form expressions for the CR bound because of the matrix inversion involved. Therefore, only numerical analysis is given in this paper to investigate the influence of the current frequency on the CR bounds. To this end, a Samsung 18 650 Lithium battery cell is studied in this paper. The static capacity test and hybrid pulse test are conducted at 20 °C to determine the values of parameters. The specifications and main parameters of the chosen battery cell are listed in Table I. We point out that R_s, R_t, and τ change with varying SoC. However, in the CR bound analysis, only the nominal values R_s, R_t, and τ, listed in Table I, are used for simplification.

As shown in Fig. 3, the OCV-SoC curve can be linearized over the SoC range of 50%–90% and the slope used in the CR bound analysis is 8.845 mV/100%. The coefficients K_{0-4} in the OCV-SoC curve are specified in Table II.

To compare the CR bounds of two estimation scenarios, the current waveform including two sinusoidal components [see (24)] is also used to calculate the CR bounds for single-parameter estimation.

TABLE II
COEFFICIENTS OF THE OCV-SoC CURVE

Coefficient	Value
K_0	2.6995
K_1	0.0574
K_2	-1.3967
K_3	-0.5508
K_4	-0.0377

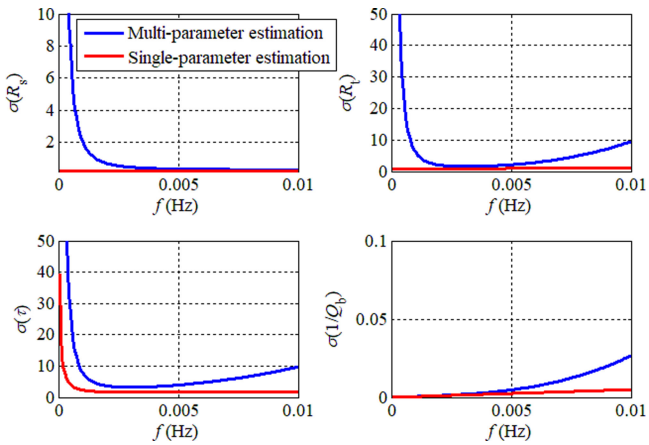

Fig. 4. CR bounds of single-parameter and multi-parameter estimations.

The numerical results are depicted in Fig. 4, and several observations are summarized as follows.

Remark 6: For R_s, R_t, τ, and $1/Q_b$, the estimation accuracy of single-parameter estimation are always higher than that of multi-parameter estimation. However, the estimation error of multi-parameter estimation is very sensitive to frequency, and it can be significantly reduced by choosing sinusoids of optimal frequency.

Remark 7: For multi-parameter estimation, there are optimal frequencies for R_t and τ estimations (the optimal frequencies for R_t and τ are slightly different, and both low).

Remark 8: There is a tradeoff between the estimation of R_s and $1/Q_b$ since the estimation of R_s prefers high-frequency current, while the estimation of $1/Q_b$ prefers low-frequency current.

For the studied battery cell, the optimal current frequency can be chosen at 0.002 Hz (5ω is therefore 0.01 Hz), since the CR bound of R_s does not significantly decrease when the frequency is higher than 0.002 Hz. Due to the space limitations, the analysis considering other frequency sets (e.g., ω and 10ω) is not presented, but we note that the results are similar.

A constant temperature is assumed in the CR bound analysis. However, temperature heavily affects the impedance values and the battery degradation behavior. We point out that, when the external temperature is constant the analysis/results can be directly generalized, although parameters of the battery change significantly under different temperatures. When the temperature changes, the CR bounds of the estimated parameters may also change, and the optimal frequency components in the current waveform, therefore, change as well. In this case, the CR

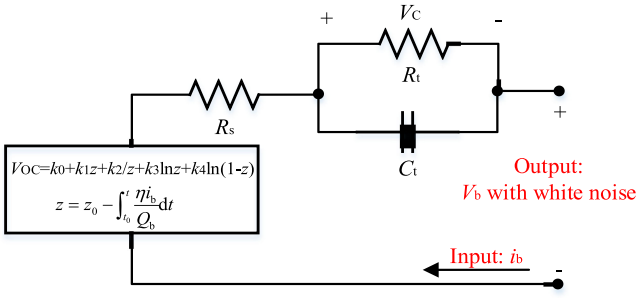

Fig. 5. Simulation model of the first-order circuit.

bounds of estimated parameters can be derived considering different parameters' values related to different temperatures. As a result, the optimal frequency components, which are injected online to improve the parameter estimation performance, can be determined for different temperatures offline. In general, the battery temperature does not change quickly due to its large thermal capacity. However, for the extreme case where the battery temperature does change quickly, it is difficult to directly generalize the results in this paper, since the battery parameters are assumed to be constant in the CR bound analysis. Parameter estimation will be more difficult in this case because the estimation algorithm needs to handle not only the erroneous initial guesses of the estimated parameters, but also the parameter dynamics related to the temperature change.

IV. Simulation Results

Most previous studies directly use experiments to validate the battery states/parameters estimation algorithm. However, we point out that the estimation error comes from the following three aspects:

1) The limitation of the battery model.
2) The limitation of the estimation algorithm.
3) The inherent limitation of the estimation problem formulation.

In this paper, the error from the estimation algorithm is not considered, as the adopted multi-scale EKF has been verified to have satisfactory performance [16]. This paper investigates the influence of the battery current waveform on estimation accuracy. To remove errors from the battery model limitation, a simulation is conducted to verify the CR bound analysis results, which cannot be realized in experiments.

As shown in Fig. 5, the simulation is conducted based on the first-order ECM whose voltage is governed by the same dynamics as the battery cell adopted in this study [i.e., (2) and (3)]. The parameters R_s, R_t, and τ are set to vary with SoC (i.e., z) based on the hybrid pulse power characterization (HPPC) results of the Samsung battery to examine whether both the initial parameters/states errors and system dynamics can be handled simultaneously. In this case, the battery model limitation does not exist because we estimate the parameter of the first-order ECM rather than the battery cell.

The CR bound analysis in Section III-C focuses on four parameters, but the real estimation focuses on six states/parameters in total. To satisfy the PE condition, for the optimal current

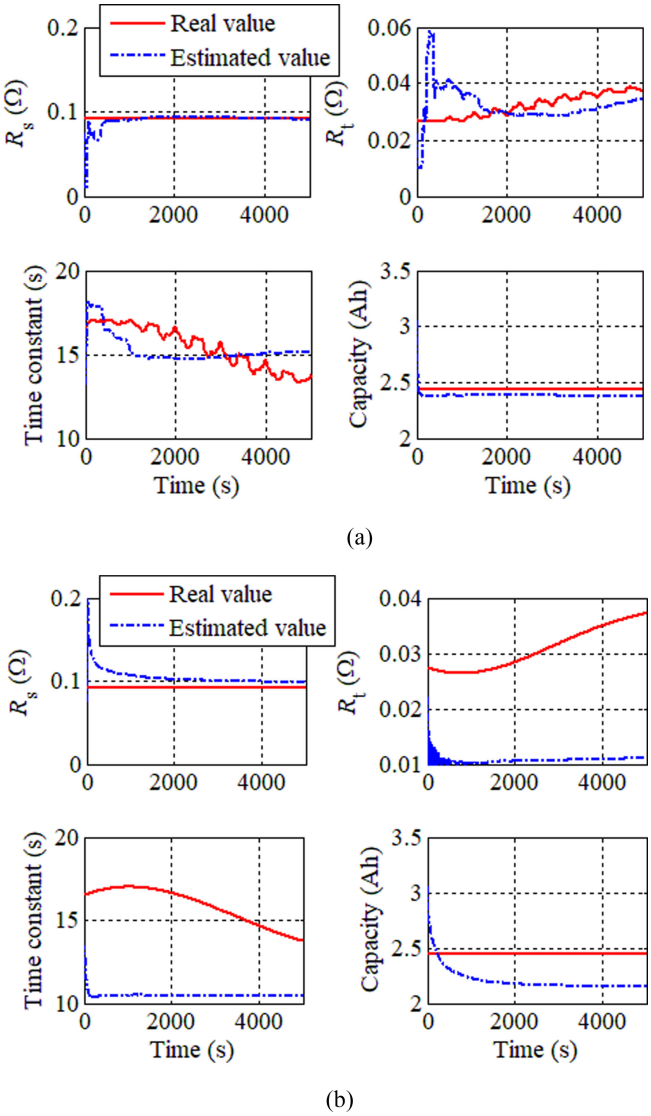

Fig. 6. Simulation results of parameter estimation. (a) Results with optimal current profile. (b) Results with non-optimal current profile.

profile, three sine waves with frequencies of 0.002, 0.01, and 0.005 Hz (an additional component) are adopted. For the comparison, in the second simulation, the frequencies of the sine waves increase to 0.02, 0.05, and 0.1 Hz. The amplitudes of all sine waves are set at 0.5 C (1.22 A). The time scale ratio L in the multi-scale EKF is chosen to be 5 s for all simulations and experiments. In the simulation, the initial guess of the parameters is set to 80% of the real value, and the initial guess of the state is set to $[V_C(0,0)\ z(0,0)]^{\mathrm{T}} = [\,0\ 1\,]^{\mathrm{T}}$.

As shown in Fig. 6(a), when the optimal current waveform is used, the estimated R_s quickly converges to the actual value, and there is hardly any error. For R_t and τ, the estimated parameters can by-and-large track the actual values. The estimated battery capacity converges to the real value, but there is a small static error (i.e., 0.05 Ah, or 2%). In contrast, as shown in Fig. 6(b), when the non-optimal current is used, the estimated values of R_t and τ cannot track their actual values at all, and the static error in the estimated Q_b significantly increases, although the estimation

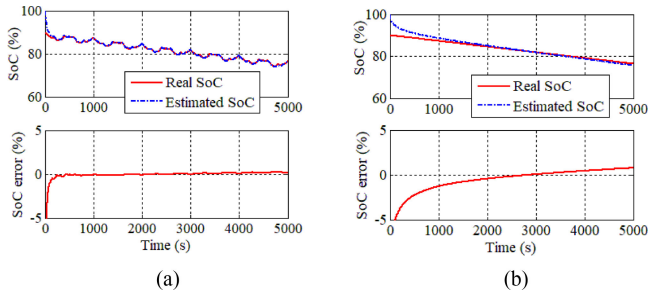

Fig. 7. Simulation results of SoC estimation. (a) Optimal current profile. (b) Non-optimal current profile.

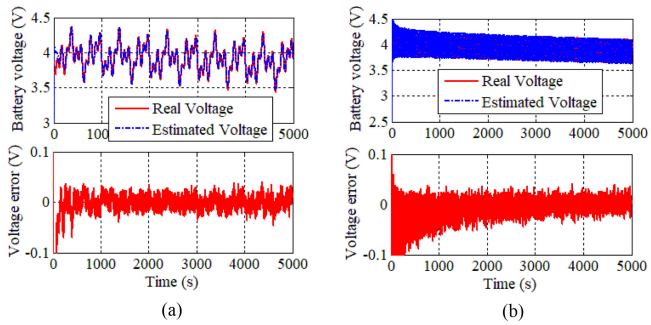

Fig. 8. Simulation results of V_b estimation. (a) Optimal current profile. (b) Non-optimal current profile.

result of R_s is still satisfactory. In addition, it shows that the estimated R_t and τ cannot accurately track the trajectories of the real values, even though the optimal current profile is used. We point out that the errors in R_t and τ are also caused by limitations of the estimation problem itself. As shown in Fig. 6, the diffusion resistance R_t is much smaller than the ohmic resistance R_s. Thus, when compared to R_s, the influence of R_t and τ on the battery terminal voltage is small. Consequently, it is difficult to estimate R_t and τ accurately when an estimation of R_s is also included.

As shown in Fig. 7(a), the estimated SoC follows the real value accurately and quickly when the optimal current profile is used, though significant initial error exists, and the SoC estimation error is less than 0.5%. However, since the estimated battery capacity directly influences the estimation of SoC, the estimated SoC becomes worse when the non-optimal current profile is used, as shown in Fig. 7(b).

Since all parameters and states can be accurately estimated when the optimal current profile is used, the estimated voltage follows the true voltage very well and the estimated error is less than 0.05 V, as shown in Fig. 8(a). It is interesting to see that, when the current frequency increases, the estimation error of the voltage does not significantly increase, as shown in Fig. 8(b). The reason is that a local minimum is achieved and the estimation errors of SoC and Q_b compensate their influences on the terminal voltage. In addition, the RC pair has a negligible influence on voltage, therefore, the estimated voltage can track the real value even when the estimated R_t and τ are far from the real values. The simulation results in this section quantify the estimation error mainly caused by the estimation problem itself. Thus, the CR bound analysis result in Section III-C is

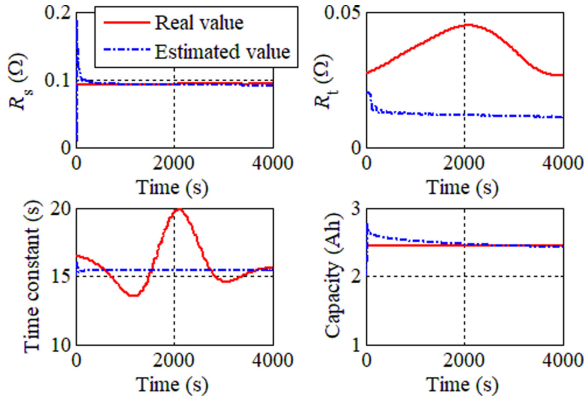

Fig. 9. Experimental result of parameter estimation with optimal battery current.

demonstrated. The estimation performance can be significantly improved when the optimal current profile is used.

V. Experimental Results

The experiments use a Samsung 18 650 Lithium ion battery, whose specifications are listed in Table I. Besides error from the estimation problem itself, the error caused by the inaccuracy of the first-order ECM is also involved in the experiment. The simulation results in Section IV show that, when the ECM parameters are similar to the "true values" of the studied battery, the RC pair is difficult to characterize, even when the optimal battery current profile is used. Thus, the parameters of the RC pair are more difficult to be estimated in experiment. In addition, the optimal frequency for R_t and τ estimations, which are pretty low, will result in a long time before parameters are estimated, hence there is a tradeoff between estimation accuracy and speed. In the first experiment, the optimal current profile, including three sine waves with frequencies of 0.01, 0.05, and 0.1 Hz, is employed. In the following experiment, the initial guess of the parameters are set to $[R_s(0)\, R_t(0)\, \tau(0)\, 1/\, Q_b(0)]^{\mathrm{T}} = [0.06\, 0.02\, 15\, 1/\, 2]^{\mathrm{T}}$, and the initial guess of the state is set to $[V_C(0, 0)\, z(0, 0)]^{\mathrm{T}} = [\,0\, 0.4]^{\mathrm{T}}$. The parameter estimation results are shown in Fig. 9, showing that the estimated R_s converges quickly to the real value; however, for R_t and τ, the estimated parameters cannot track the "actual values." Along with the simulation results, it can be concluded that the RC parameters are difficult to be estimated for the studied battery cell. The reasons are that are as follows: First, the influence of RC pair dynamics on the battery terminal voltage is negligible, and second, the first-order ECM cannot represent the battery dynamics precisely.

The estimated battery capacity can converge to the real value, which takes about 2000 s. The errors in R_t and τ are mainly caused by the limitations of the estimation problem and the first-order RC model. It is difficult to ascertain how accurate the R_t and τ values from the HPPC test are. When compared to the simulation results, the SoC estimation result of the experiment is worse, as shown in Fig. 10. In addition, the steady-state estimation error in the battery terminal voltage is also slightly larger due to the limitations of the first-order RC model.

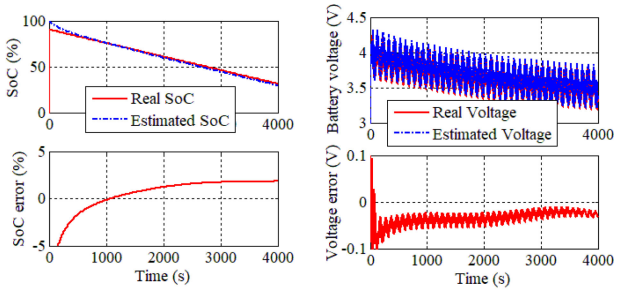

(a) (b)

Fig. 10. Experimental result of SoC and V_b estimations with optimal battery current. (a) SoC. (b) V_b.

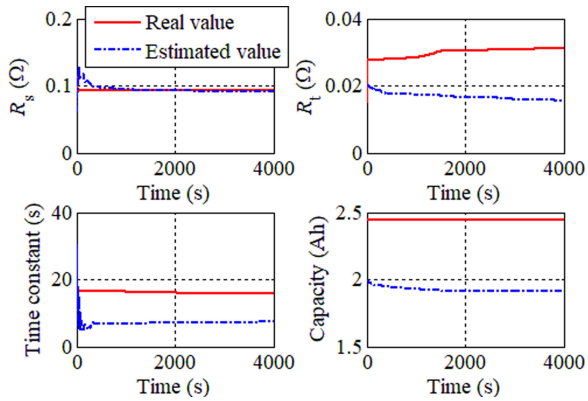

Fig. 11. Experimental result of parameter estimation under NEDC.

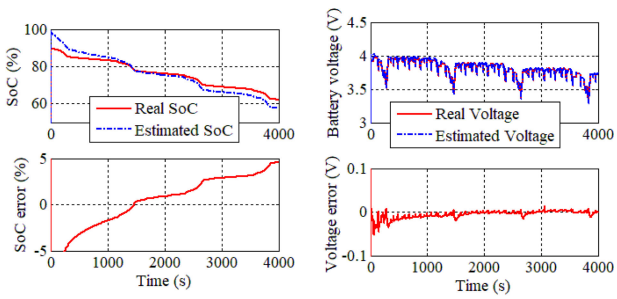

(a) (b)

Fig. 12. Experimental result of SoC and V_b estimations under NEDC. (a) SoC. (b) V_b.

To present the influence of the current profile on estimation performance, another experiment based on the scaled New European Driving Cycle (NEDC), which contains higher frequency currents than the optimal profile, is also conducted. The parameter estimation result is shown in Fig. 11, which shows that R_s converges to the actual value accurately and quickly. The CR bound analysis result that the estimation of R_s prefers high frequency is verified. Both the estimations of SoC, R_t, τ, and Q_b are compromised due to the high-frequency current of the NEDC. The estimated battery capacity converges to the wrong value, which may be due to a local minimum for the estimation problem, which also induces a low estimation error of battery terminal voltage, as shown in Fig. 12(b). Therefore, the experimental results in this section validate that the battery SoC/SoH estimation performance can be significantly improved by injecting the optimal current profile.

Based on observations from the simulation and experiment, it can be found that the current waveform is critical to battery states and parameters estimation. We point out that the battery parameters vary over a large range depending on the chemistry. However, the CR bound analysis in this paper presents quantitative insights of the combined SoC/SoH estimation based on the ECM, and provides important guidelines on designing the optimal current profile for a better estimation performance.

For electric vehicles, it is difficult to design the battery current profile, since battery is the sole power source onboard and needs to supply the power demand throughout. However, batteries are often used in over-actuated systems, e.g., the hybrid electric vehicle [44] and the hybrid energy storage system [45]. These over-actuated systems offer an additional degree of freedom to generate excitation currents for battery to achieve better parameters/states estimation performance. Thus, the optimal current profile can be directly used in these applications.

VI. Discussion

As shown in Figs. 9 and 10, the estimation process takes a significant amount of time to make the estimated parameters/states converge, even though the optimal current profile is adopted. The long estimation time is inherently caused by the estimation problem itself, since many parameters/states (i.e., four parameters and two states) are estimated simultaneously, while only one input (i.e., current) and one output (i.e., terminal voltage) are available. Therefore, there are many local minimums in the estimation process, which make the estimation algorithm difficult to obtain the expected global minimum. The long estimation time has also been noticed in the existing literature [16], and it takes even more time without the injection of optimal current signals. If the battery is the only power source, it is true that one cannot vary the power demand to satisfy parameter estimation requirements without negative consequences. The best way to inject the optimal current signals is by manipulating the battery charging profile, since it has much less negative consequences when the battery is being charged. However, when the battery is used in an over-actuated system (e.g., hybrid electric vehicle), which has multiple power sources that provide the ability to achieve sufficiently rich input signals and output regulation objectives simultaneously, the long period of estimation may not interrupt the application. For any power demand P_d, we have $P_d = P_{s1} + P_{s2}$, where P_{s1} and P_{s2} are the power from source 1 (e.g., battery) and source 2 (e.g., engine). The optimal current waveform for identification can be designed for one source, while the other source can be used to deliver the power demand and eliminate the negative consequences of the excitation.

For the frequency ratio, we have performed some simulations and selected the optimal ratio based on the CR bound analysis. The frequency ratio k in the current signal, which is used in the CR bound analysis, can be defined as

$$i_b(t) = M\cos(\omega t) + M\cos(k\omega t). \tag{26}$$

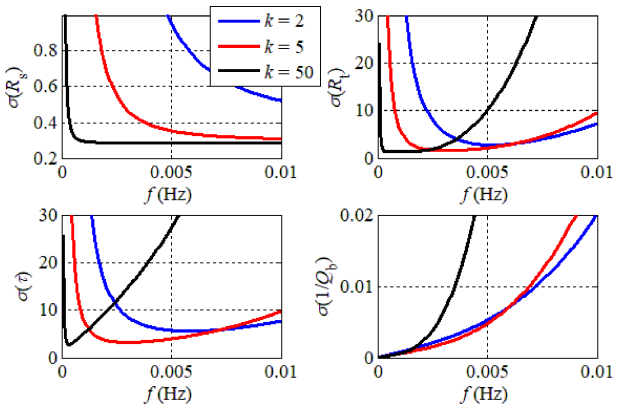

Fig. 13. CR bound results under different frequency ratios.

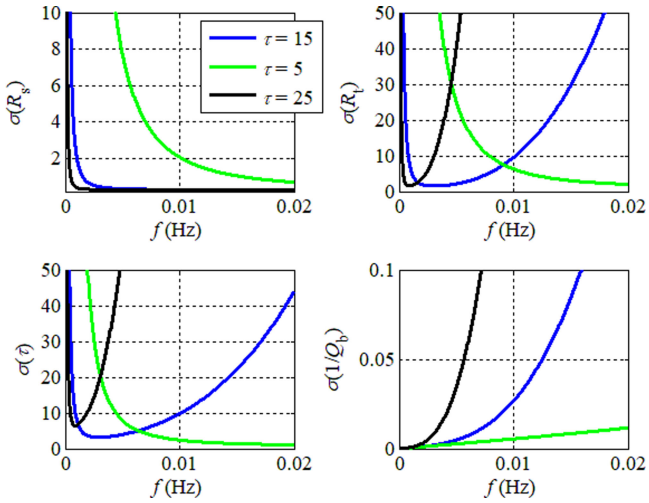

Fig. 14. CR bound results under different τ values.

In the CR bound analysis shown in Section III, k is chosen to be 5. This is based on the CR bound results, as shown in Fig. 13. The CR bounds of the estimated parameters under $k = 2$, 5, and 50 show that the best performance can be achieved in the "optimal frequency range (around 0.002 Hz)" when k is 5. When k is extremely low (i.e., 2), the CR bound of R_s is much higher than others due to the lack of high-frequency current component. In contrast, when k is extremely high (i.e., 50), the CR bound of R_s is significantly reduced, however, the CR bounds of R_t, τ, and Q_b are dramatically increased, since they prefer low-frequency current components. As a result, k cannot be too low or too high to achieve satisfactory estimation performance.

We did not investigate all k values because another frequency component is added in both the simulation and the experiment, while the CR bound analysis only adopts the current signal consisting of two frequency components. When the third frequency component, which is used to achieve the PE condition, is added in (26), the CR bound analysis will be very complicated, and even the numerical result is hard to be obtained. Consequently, the third frequency components of both simulation and experiment are randomly chosen without the loss of generality.

In addition, fixed parameters are assumed in the CR bound analysis, while the actual nominal values of the ECM parameters change significantly with the battery SoC. The nominal parameters used in the CR bound analysis are the average values over the SoC operation range, and the nominal values are calibrated through HPPC using the recursive least-squares method.

We point out that current frequencies that are considered to be non-optimal in the CR bound analysis and simulations (i.e., 0.01, 0.05, and 0.1 Hz) are selected as optimal values for experiments. The reasons are listed as follows:

1) In the CR bound analysis, all battery parameters are considered to be constant. However, the parameters, especially the parameters of RC pair, significantly change with the battery SoC, as shown in Fig. 9. The parameter variation influences the CR bound result, and therefore, results in different optimal frequency components. For example, when τ changes and the other parameters remain constant (as listed in Table I), the CR bounds of different estimated parameters significantly change, as shown in Fig. 14. It is intuitive that small τ prefers high-frequency current, and vice versa. In the simulation, the SoC operating range is narrow (i.e., 75%–90%), thus, the battery parameters are relatively constant and near to the values used in the CR bound analysis provided in Section III. As a result, the optimal current signals derived from the CR bound analysis can be directly used in the simulation. In contrast, battery parameters change dramatically in the experiment because the SoC operation range is wide (i.e., 35%–90%). Considering the parameter variations of the RC pair, we slightly increase the optimal frequencies of the current waveform from 0.002 and 0.01 Hz (derived from CR bound analysis) to 0.01 and 0.05 Hz.
2) The first-order ECM does not perfectly represent the battery dynamics. Hence, the optimal current waveform derived from the CR bound analysis can be directly used in the simulation, since the dynamics of the first-order ECM is studied. However, in the experiment, the inaccuracy of the first-order ECM is involved, therefore, the optimal frequencies of battery current will change when compared to the CR bound analysis to adapt to the actual battery dynamics.

VII. Conclusion

This paper presents a combined SoC/SoH estimation of a Lithium ion battery based on a first-order ECM. A multi-scale EKF is adopted to estimate battery parameters and states using dual time scales. Considering voltage noise, current amplitude, and current frequency, a CR bound analysis is conducted to quantify the influence of the current profile on estimation accuracy. Several important observations were made, such as the following.

1) CR bounds of SoC for both single-parameter and multi-parameter estimations are the same and only depend on measurement noise and OCV slope.
2) For R_s, R_t, τ, and $1/Q_b$, the estimation accuracy of single-parameter estimation is higher than that of multi-parameter estimation.

3) The CR bound of R_s monotonically decreases with increasing current frequency.
4) For multi-parameter estimation, there are optimal frequencies for R_t and τ estimations.
5) The estimation accuracy of $1/Q_b$ can be improved by decreasing the current frequency. Therefore, the optimal current profile can be designed based on CR bound analysis results.

Both simulation and experimental results verify the CR bound analysis and show that the battery current profile with optimal frequency components achieves satisfactory estimation performance. The CR bound analysis in this paper presents quantitative insights into the SoC/SoH estimation problem when a first-order ECM is adopted. In this experiment, the estimation result with the optimal current profile is much better than the one under NEDC. Thus, the CR bound analysis in this paper provides important guidelines on designing the optimal current waveform for a better performance for online estimation and offline calibration.

REFERENCES

[1] L. Lu, X. Han, J. Li, J. Hua, and M. Ouyang, "A review on the key issues for lithium-ion battery management in electric vehicles," *J. Power Sources*, vol. 226, pp. 272–288, Mar. 2013.

[2] J. Zhang and J. Lee, "A review on prognostics and health monitoring of Li-ion battery," *J. Power Sources*, vol. 196, pp. 6007–6014, Aug. 2011.

[3] X. Han, M. Ouyang, L. Lu, J. Li, Y. Zheng, and Z. Li, "A comparative study of commercial lithium ion battery cycle life in electrical vehicle: Aging mechanism identification," *J. Power Sources*, vol. 251, pp. 38–54, Apr. 2014.

[4] Y. Çadırcı and Y. Özkazanç, "Microcontroller-based on-line state-of-charge estimator for sealed lead–acid batteries," *J. Power Sources*, vol. 129, no. 2, pp. 330–342, 2004.

[5] M. Charkhgard and M. Farrokhi, "State-of-charge estimation for lithium-ion batteries using neural networks and EKF," *IEEE Trans. Ind. Electron.*, vol. 57, no. 12, pp. 4178–4187, Dec. 2010.

[6] X. Lin *et al.*, "A lumped-parameter electro-thermal model for cylindrical batteries," *J. Power Sources*, vol. 257, pp. 1–11, Jul. 2014.

[7] W. Gu and C. Wang, "Thermal-electrochemical modeling of battery systems," *J. Electrochem. Soc.*, vol. 147, no. 8, pp. 2910–2922, 2000.

[8] X. Hu, S. Li, and H. Peng, "A comparative study of equivalent circuit models for Li-ion batteries," *J. Power Sources*, vol. 198, pp. 359–367, Jan. 2012.

[9] K. Ng, C. Moo, Y. Chen, and Y. Hsieh, "Enhanced coulomb counting method for estimating state-of-charge and state-of-health of lithium-ion batteries," *Appl. Energy*, vol. 86, no. 9, pp. 1506–1511, Sep. 2009.

[10] Y. Zheng, M. Ouyang, L. Lu, J. Li, Z. Zhang, and X. Li, "Study on the correlation between state of charge and coulombic efficiency for commercial lithium ion batteries," *J. Power Sources*, vol. 289, pp. 81–90, Sep. 2015.

[11] G. Plett, "Extended Kalman filtering for battery management systems of LiPB-based HEV battery packs: Part 3. State and parameter estimation," *J. Power Sources*, vol. 134, no. 2, pp. 277–292, Aug. 2004.

[12] F. Sun, X. Hu, Y. Zou, and S. Li, "Adaptive unscented Kalman filtering for state of charge estimation of a lithium-ion battery for electric vehicles," *Energy*, vol. 36, no. 5, pp. 3531–3540, May 2011.

[13] F. Zhang, G. Liu, L. Fang, and H. Wang, "Estimation of battery state of charge with H∞ observer: Applied to a robot for inspecting power transmission lines," *IEEE Trans. Ind. Electron.*, vol. 59, no. 2, pp. 1086–1095, Feb. 2012.

[14] I. Kim, "The novel state of charge estimation method for lithium battery using sliding mode observer," *J. Power Sources*, vol. 163, no. 1, pp. 584–590, Dec. 2006.

[15] A. Zenati, P. Desprez, and H. Razik, "Estimation of the SOC and the SOH of Li-ion batteries, by combining impedance measurements with the Fuzzy logic inference," in *Proc. 36th Annu. Conf. IEEE Ind. Electron. Soc.*, 2010, pp. 1773–1778.

[16] R. Xiong, F. Sun, Z. Chen, and H. He, "A data-driven multi-scale extended Kalman filtering based parameter and state estimation approach of lithium-ion olymer battery in electric vehicles," *Appl. Energy*, vol. 113, pp. 463–476, Jan. 2014.

[17] P. Rong and M. Pedram, "An analytical model for predicting the remaining battery capacity of lithium-ion batteries," *IEEE Trans. Very Large Scale Integration Syst.*, vol. 14, no. 5, pp. 441–451, Jul. 2006.

[18] H. He, R. Xiong, X. Zhang, F. Sun, and J. Fan, "State-of-charge estimation of the lithium-ion battery using an adaptive extended Kalman filter based on an improved Thevenin model," *IEEE Trans. Veh. Technol.*, vol. 60, no. 4, pp. 1461–1469, Mar. 2011.

[19] H. Rahimi-Eichi, F. Baronti, and M. Chow, "Online adaptive parameter identification and state-of-charge coestimation for lithium-polymer battery cells," *IEEE Trans. Ind. Electron.*, vol. 61, no. 4, pp. 2053–2061, May 2013.

[20] B. Suthar *et al.*, "Optimal control and state estimation of lithium-ion batteries using reformulated models," in *Proc. Amer. Control Conf.*, 2013, pp. 5350–5355.

[21] S. Dey, B. Ayalew, and P. Pisu, "Nonlinear robust observers for state-of-charge estimation of lithium-ion cells based on a reduced electrochemical model," *IEEE Trans. Control Syst. Technol.*, vol. 23, no. 5, pp. 1935–1942, Jan. 2015.

[22] E. Wan and A. Nelson, "Dual extended Kalman filter methods," in *Kalman Filtering and Neural Networks*. Hoboken, NJ, USA: Wiley, 2002, pp. 123–173.

[23] C. Hu, B. Youn, and J. Chung, "A multiscale framework with extended Kalman filter for lithium-ion battery SOC and capacity estimation," *Appl. Energy*, vol. 92, pp. 694–704, Apr. 2012.

[24] X. Lin, "Analytic analysis of the data-dependent estimation accuracy of battery equivalent circuit dynamics," *IEEE Contr. Syst. Lett.*, vol. 1, no. 2, pp. 304–309, Jun. 2017.

[25] P. Ioannou and J. Sun, *Robust Adaptive Control*, vol. 1. North Chelmsford, MA, USA: Courier Corporation, 2012.

[26] A. Klintberg, T. Wik, and B. Fridholm, "Theoretical bounds on the accuracy of state and parameter estimation for batteries," in *Proc. Amer. Control Conf.*, 2017, pp. 4035–4041.

[27] M. Rothenberger, D. Docimo, M. Ghanaatpishe, and H. Fathy, "Genetic optimization and experimental validation of a test cycle that maximizes parameter identifiability for a Li-ion equivalent-circuit battery model," *J. Energy Storage*, vol. 4, pp. 156–166, Dec. 2015.

[28] M. Rothenberger, J. Anstrom, S. Brennan, and H. Fathy, "Maximizing parameter identifiability of an equivalent-circuit battery model using optimal periodic input shaping," in *Proc. ASME Dyn. Syst. Control Conf.*, 2014, pp. V001T19A004-1–V001T19A004-10.

[29] X. Lin and A. Stefanopoulou, "Analytic bound on accuracy of battery state and parameter estimation," *J. Electrochem. Soc.*, vol. 162, no. 9, pp. A1879–A1891, 2015.

[30] X. Lin, "Theoretical analysis of battery SOC estimation errors under sensor bias and variance," *IEEE Trans. Ind. Electron.*, vol. 65, no. 9, pp. 7138–7148, Sep. 2018.

[31] Y. Zheng, M. Ouyang, X. Han, L. Lu, and J. Li, "Investigating the error sources of the online state of charge estimation methods for lithium-ion batteries in electric vehicles," *J. Power Sources*, vol. 377, pp. 161–188, Feb. 2018.

[32] Z. Song, J. Hou, H. Hofmann, X. Lin, and J. Sun, "Parameter identification and maximum power estimation of battery/supercapacitor hybrid energy storage system based on Cramer-Rao bound analysis," *IEEE Trans. Power Electron.*, to be published, doi: 10.1109/TPEL.2018.2859317.

[33] Y. Zheng *et al.*, "Cell state-of-charge inconsistency estimation for LiFePO4 battery pack in hybrid electric vehicles using mean-difference model," *Appl. Energy*, vol. 111, pp. 571–580, Nov. 2013.

[34] C. Weng, Y. Cui, J. Sun, and H. Peng, "On-board state of health monitoring of lithium-ion batteries using incremental capacity analysis with support vector regression," *J. Power Sources*, vol. 235, pp. 36–44, Aug. 2013.

[35] J. Wei, G. Dong, and Z. Chen, "Remaining useful life prediction and state of health diagnosis for lithium-ion batteries using particle filter and support vector regression," *IEEE Trans. Ind. Electron.*, vol. 65, no. 7, pp. 5634–5643, Jul. 2018.

[36] D. Andre, C. Appel, T. Soczka-Guth, and D. Sauer, "Advanced mathematical methods of SOC and SOH estimation for lithium-ion batteries," *J. Power Sources*, vol. 224, pp. 20–27, Feb. 2013.

[37] Z. Guo, X. Qiu, G. Hou, B. Liaw, and C. Zhang, "State of health estimation for lithium ion batteries based on charging curves," *J. Power Sources*, vol. 249, pp. 457–462, Mar. 2014.

[38] Y. Zou, X. Hu, H. Ma, and S. Li, "Combined state of charge and state of health estimation over lithium-ion battery cell cycle lifespan for electric vehicles," *J. Power Sources*, vol. 273, pp. 793–803, Jan. 2015.
[39] H. Dai, and X. Wei, Z. Sun, J. Wang, and W. Gu, "Online cell SOC estimation of li-ion battery packs using a dual time-scale Kalman filtering for EV applications," *Appl. Energy*, vol. 95, pp. 227–237, Jul. 2012.
[40] X. Lin, "On the analytic accuracy of battery SOC, capacity and resistance estimation," in *Proc. Amer. Control Conf.*, 2016, pp. 4006–4011.
[41] L. Scharf and L. McWhorter, "Geometry of the Cramer-Rao bound," *Signal Process.*, vol. 31, no. 3, pp. 301–311, 1993.
[42] X. Hu, F. Sun, and Y. Zou, "Estimation of state of charge of a lithium-ion battery pack for electric vehicles using an adaptive Luenberger observer," *Energies*, vol. 3, no. 9, pp. 1586–1603, 2010.
[43] N. Samad, J. Siegel, and A. Stefanopoulou, "Parameterization and validation of a distributed coupled electro-thermal model for prismatic cells," in *Proc. ASME Dyn. Syst. Control Conf.*, 2014, pp. V002T23A006-1–V002T23A006-9.
[44] Z. Song, X. Zhang, J. Li, H. Hofmann, M. Ouyang, and J. Du, "Component sizing optimization of plug-in hybrid electric vehicles with the hybrid energy storage system," *Energy*, vol. 144, pp. 393–403, Feb. 2018.
[45] Z. Song, J. Hou, S. Xu, M. Ouyang, and J. Li, "The influence of driving cycle characteristics on the integrated optimization of hybrid energy storage system for electric city buses," *Energy*, vol. 135, pp. 91–100, Sep. 2017.

Ziyou Song (M'18) received the B.E. (hons.) and the Ph.D. degrees (highest hons.) in automotive engineering from Tsinghua University, Beijing, China, in 2011 and 2016, respectively.

He is currently a Postdoctor with the University of Michigan, Ann Arbor, MI, USA. His research interests include battery parameter estimation, hybrid energy storage systems, and electric and hybrid electric vehicles.

Xiaogang Wu was born in Hegang, China. He received the M.E. and Ph.D. degrees in power electronics and power transmission from the Harbin University of Science and Technology, Harbin, China, in 2006 and 2009, respectively.

From 2010 to 2012, he was a Postdoctoral Researcher with Tsinghua University, Beijing, China. He is currently a Professor with the Harbin University of Science and Technology, Harbin. His research interests include optimization matching and energy management of hybrid power systems, power battery charge management, and electric vehicle access technology.

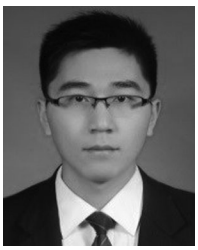

Xuefeng Li was born in Weifang, China. He received the B.E. degree in electrical engineering and automation from the Qingdao University of Technology, Qingdao, China, in 2014. He is currently working toward the M.E. degree in electrical engineering at the Harbin University of Science and Technology, Harbin, China.

His research mainly focuses on the battery management system in electric vehicles.

Jing Sun (M'89–SM'00–F'04) received the B.S. and M.S. degrees from the University of Science and Technology of China, Hefei, China, in 1982 and 1984, respectively, and the Ph.D. degree from the University of Southern California, Los Angeles, CA, USA, in 1989.

From 1989 to 1993, she was an Assistant Professor with the Department of Electrical and Computer Engineering, Wayne State University. She joined Ford Research Laboratory, in 1993, where she was with the Powertrain Control Systems Department. After spending almost 10 years in industry, she came back to academia and joined the faculty of the College of Engineering, University of Michigan, in 2003, where she is currently a Michael G. Parsons Professor and the Chair with the Department of Naval Architecture and Marine Engineering, with courtesy appointments as a Professor with the Department of Electrical Engineering and Computer Science and the Department of Mechanical Engineering. Her research interests include system and control theory and its applications to marine and automotive propulsion systems. She holds 39 US patents and has coauthored a textbook on *Robust Adaptive Control*. She is a recipient of the 2003 IEEE Control System Technology Award.

Heath F. Hofmann (S'90–M'92–SM'16) received the Ph.D. degree in electrical engineering and computer science from the University of California at Berkeley, Berkeley, CA, USA, in 1998.

He is currently a Professor with the University of Michigan, Ann Arbor, MI, USA. He has authored approximately four dozen papers in refereed journals. He currently holds 14 patents. His research interests include power electronics, specializing in the design, simulation, and control of electromechanical systems, adaptive control techniques, energy harvesting, flywheel energy storage systems, electric and hybrid electric vehicles, and finite-element analysis.

Jun Hou (S'15–M'18) received the M.S. degrees in electrical engineering from Northeastern University, Shenyang, China, in 2011, the Ph.D. degree from the University of Michigan, Ann Arbor, MI, USA, in 2017.

His current research interests include integration, modeling, control, and optimization of hybrid energy storage, power electronic converters and electric propulsion systems.